CHEMISTRY OF MATERIALS
Cite This: Chem. Mater. 2019, 31, 1761−1766
Article
pubs.acs.org/cm

Ultrahigh Vacuum Self-Assembly of Rotationally Commensurate C8-BTBT/MoS_2/Graphene Mixed-Dimensional Heterostructures

Xiaolong Liu,[†] Itamar Balla,[‡] Vinod K. Sangwan,[‡] Hakan Usta,[§] Antonio Facchetti,[∥] Tobin J. Marks,[†,‡,∥] and Mark C. Hersam*[,†,‡,∥,⊥]

[†]Applied Physics Graduate Program, [‡]Department of Materials Science and Engineering, [∥]Department of Chemistry, and [⊥]Department of Electrical Engineering and Computer Science, Northwestern University, Evanston, Illinois 60208, United States

[§]Department of Materials Science and Nanotechnology Engineering, Abdullah Gül University, 38080 Kayseri, Turkey

Supporting Information

ABSTRACT: Mixed-dimensional van der Waals heterostructures combine the advantages of nanomaterials with qualitatively distinct properties such as the extended bandstructures and high charge carrier mobilities of inorganic two-dimensional materials and the discrete orbital energy levels and strong optical absorption of zero-dimensional organic molecules. The synergistic interplay between nanomaterials of distinct dimensionality has enabled a variety of unique applications such as antiambipolar transistors, sensitized photodetectors, and gate-tunable photovoltaics. Because the performance of mixed-dimensional heterostructure devices depends sensitively on the buried interfacial structure, it is of great interest to identify materials and chemistries that naturally form highly ordered heterointerfaces. Toward this end, here we demonstrate ultrahigh vacuum self-assembly of 2,7-dioctyl[1]benzothieno[3,2-*b*][1]benzothiophene (C8-BTBT) monolayers onto epitaxial MoS_2/graphene heterostructures. With molecular-resolution scanning tunneling microscopy and spectroscopy, the resulting C8-BTBT/MoS_2/graphene mixed-dimensional heterostructures are found to be rotationally commensurate with well-defined physical and electronic structures. It is further shown that the self-assembled C8-BTBT monolayers are insensitive to the structural defects and electronic perturbations of the underlying MoS_2 substrate, which provides significant processing latitude. For these reasons, this work will facilitate ongoing efforts to utilize organic/MoS_2/graphene mixed-dimensional heterostructures for electronic, optoelectronic, and photovoltaic applications.

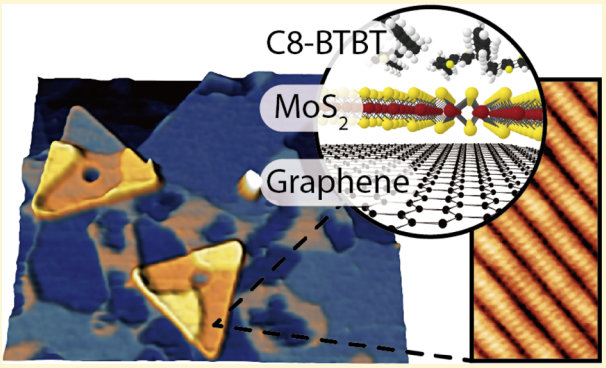

Noncovalent van der Waals interactions enable versatile integration of dissimilar materials without dangling bonds. By relaxing lattice matching constraints, van der Waals bonding not only allows vertical stacking of two-dimensional (2D) layers with clean and abrupt interfaces,[1] but also mediates effective coupling of nanomaterials with different dimensionalities.[2,3] These mixed-dimensional heterostructures[2,4] significantly expand the number of van der Waals heterostructure permutations and allow the qualitatively distinct properties of different dimensionality nanomaterials to be combined in one system. In particular, the interplay between the highly localized molecular orbitals of zero-dimensional (0D) organic molecules and the extended bandstructure of inorganic 2D materials has been exploited for proof-of-concept optoelectronic,[5,6] energy-harvesting[7,8] and light-emitting device applications.[9] In addition to desirable physical properties, the high processing throughput and potential as a seeding layer for subsequent chemistry[10] facilitates the realization of large-area organic/2D mixed-dimensional heterostructures, especially compared to all-2D heterostructures, where large-area growth has only been realized in limited cases.[11]

One of the most established families of 2D materials are the monolayer transition metal dichalcogenides (TMDCs).[12−14] Early attempts to form organic/MoS_2 mixed-dimensional heterojunctions have revealed unique charge and energy transfer in addition to promising electronic and optoelectronic device functionality.[5,7,15−17] Of particular interest has been the integration of n-type 2D MoS_2 with the 0D organic p-type semiconductor pentacene, which enabled the realization of gate-tunable photovoltaic p−n heterojunctions.[16] Time-resolved transient absorption spectroscopy subsequently showed that pentacene/MoS_2 heterojunctions possesses significantly longer charge-separated state lifetimes than typical 2D−2D heterojunctions.[18,19] While these early reports highlighted some of the unique features of 0D/2D mixed-dimensional heterostructures, the disordered nature of

Received: December 29, 2018
Revised: February 1, 2019
Published: February 12, 2019

DOI: 10.1021/acs.chemmater.8b05348
Chem. Mater. 2019, 31, 1761−1766

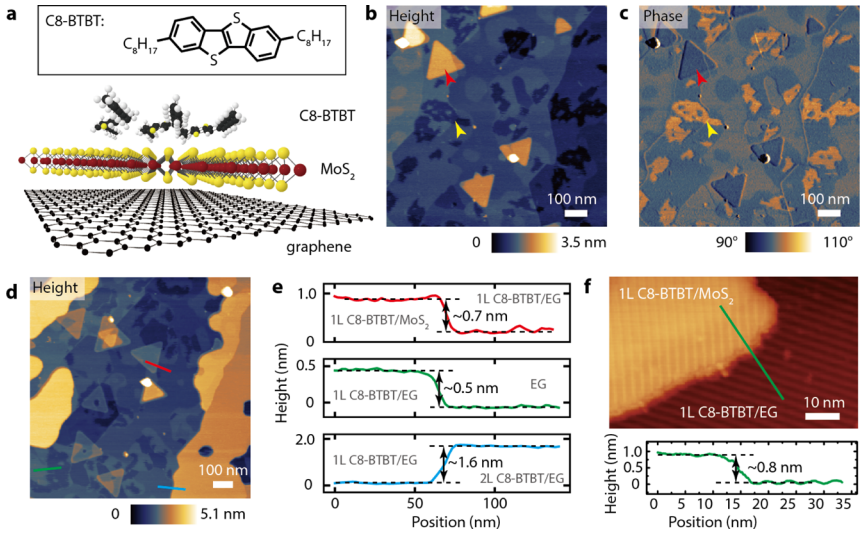

Figure 1. (a) Structure of the C8-BTBT molecule and schematic of the C8-BTBT/MoS_2/graphene mixed-dimensional heterostructure. (b) AFM height and (c) phase image of sub-monolayer C8-BTBT deposited on MoS_2/EG. The yellow and red arrow heads indicate regions corresponding to exposed graphene and monolayer MoS_2, respectively. (d) AFM height image of an area with bilayers of C8-BTBT. (e) Extracted height profiles from the corresponding traces shown in d. (f) STM image of the MoS_2/EG boundary covered by monolayer C8-BTBT. Inset: extracted height profile measured along the green line.

pentacene adlayers on MoS_2 implies an ill-defined heterointerface that ultimately limits device performance and motivates the exploration of alternative p-type organic semiconductor functionalization chemistries for MoS_2.

Among p-type organic semiconductors, 2,7-dioctyl[1]-benzothieno[3,2-*b*][1]benzothiophene (C8-BTBT) has recently attracted attention due to its high charge carrier mobility, up to 43 $cm^2\ V^{-1}\ s^{-1}$ in thin-film transistors.[20,21] In addition, C8-BTBT has been shown to form highly ordered self-assembled monolayers on 2D graphene and hexagonal boron nitride nanoflakes obtained via mechanical exfoliation, which suggests compatibility with other 2D materials.[22−25] With this motivation, here we explore the ultrahigh vacuum (UHV) assembly of C8-BTBT monolayers on epitaxial MoS_2/graphene heterostructures using molecular-resolution scanning tunneling microscopy and spectroscopy (STM/STS). The first C8-BTBT layer is found to be highly ordered in a π-face-down conformation on MoS_2 that is nearly identical to that on graphene. The orientation of C8-BTBT molecules with respect to the underlying substrate is determined, thus allowing the degree of rotational commensurability to be quantified throughout the C8-BTBT/MoS_2/graphene mixed-dimensional heterostructures. Moreover, C8-BTBT is observed to be tolerant to the underlying structural and electronic variations caused by substrate defects as evidenced by continuous C8-BTBT self-assembled monolayers over vacancies, step edges, and MoS_2 grain boundaries (GBs). This work thus establishes a methodology for forming well-defined organic/MoS_2/graphene heterointerfaces with direct implications for ongoing fundamental studies and applied technologies based on 0D/2D mixed-dimensional heterojunctions.

To avoid contamination during exfoliation, rotationally commensurate MoS_2 grown by chemical vapor deposition (CVD) on epitaxial graphene (EG) on SiC[12,26] was used for the UHV deposition of C8-BTBT. The resulting vertical C8-BTBT/MoS_2 p−n heterojunction (Figure 1a) is a prototype architecture for photodetectors, photovoltaic cells, and light-emitting diodes, where the bottom EG acts as a transparent conductor.[2,16,27−29] Sub-monolayer C8-BTBT deposited on MoS_2/EG exhibits a smooth surface morphology as shown in the atomic force microscopy (AFM) height image in Figure 1b, suggesting ordered molecular adlayers. In addition to the triangular MoS_2 domains indicated by the red arrow and terraces from EG and SiC, depressions marked by the yellow arrow are present and show enhanced contrast in the phase image of the same region (Figure 1c). This observation can be rationalized by assigning the depressions to exposed EG, whereas the rest of the surface is covered with C8-BTBT. This assignment is supported by the diffuse boundaries of the depressions when imaged at higher resolution (Figure S1a,b), which is consistent with mobile molecules found at a molecular domain boundary during AFM imaging. Figure 1d shows another area with additional layers of C8-BTBT. The step edge profiles averaged over a width of 20 pixels across a MoS_2 layer (red), a depressed region boundary (green), and a thicker C8-BTBT layer boundary (blue) are shown in Figures 1e and S2, where step heights of 0.7, 0.5, and 1.6 nm are extracted, respectively. The 0.7 nm step height corresponds well to the thickness of monolayer MoS_2, suggesting identical C8-BTBT thicknesses atop MoS_2 and EG. The 0.5 nm step height matches the reported thickness of a monolayer (1L) of C8-BTBT on graphene with a π-face-down configuration,[23] which corroborates our assignment of the depressed regions as bare EG. Finally, the 1.6 nm step height is reasonable for the second layer (2L) of C8-BTBT on graphene, which is expected to adopt a semi-standing-up configuration, where individual molecules are vertically self-assembled but with a significant tilt angle.[23]

The assumed heterostructure composed of 1L C8-BTBT on monolayer MoS_2 on EG is further confirmed by the STM image shown in Figure 1f, where rows of C8-BTBT molecules are present on both MoS_2 and EG with an expected monolayer MoS_2 step height of ∼0.8 nm. While regions of exposed EG are present for sub-monolayer C8-BTBT coverage (Figure 1b), no exposed regions of MoS_2 are detected. At higher coverages (Figure 1d), 2L C8-BTBT nucleates preferentially on 1L C8-

DOI: 10.1021/acs.chemmater.8b05348
Chem. Mater. 2019, 31, 1761−1766

BTBT/EG regions and avoids 1L C8-BTBT/MoS_2 domains as shown in Figure S1c. Preferential molecular adsorption has been observed for other 2D material systems such as borophene[30] and GaSe,[31] and can be explained by differences in the molecular adsorption enthalpies on spatially inhomogeneous substrates.

While multilayers of C8-BTBT are insufficiently conductive for stable STM imaging, the structures of 1L C8-BTBT on EG and MoS_2 are resolved at the molecular scale with UHV STM as shown in Figure 2a,b, respectively. Both structures appear as

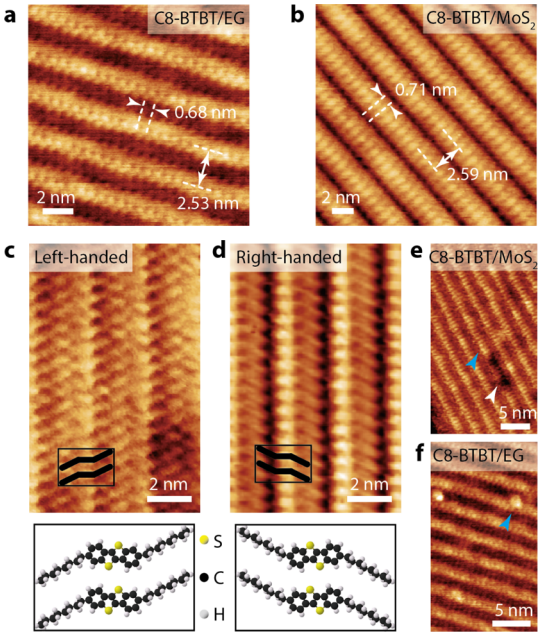

Figure 2. (a,b) STM images of self-assembled 1L C8-BTBT on (a) EG and (b) MoS_2, respectively. (c,d) STM images of two chiral structures of 1L C8-BTBT and their schematics on MoS_2. (e,f) 1L C8-BTBT self-assembles continuously over point defects (indicated by arrows) in the underlying (e) MoS_2 and (f) EG, respectively.

linear chains with similar widths (2.53 and 2.59 nm on EG and MoS_2, respectively) and periodic intra-chain segments (0.68 and 0.71 nm on EG and MoS_2, respectively), suggesting virtually identical C8-BTBT self-assembled monolayer structures on both surfaces. The measured dimensions are in agreement with the structure of 1L C8-BTBT adopting the π-face-down configuration.[24] While this result contrasts the previously reported standing-up configuration of 1L C8-BTBT on MoS_2 surfaces inferred from AFM step height measurements, the use of residue-free CVD-grown MoS_2/EG substrates and UHV processing in the present work suggests that the π-face-down configuration is preferred for the first monolayer of C8-BTBT on atomically pristine MoS_2 surfaces.[32] Higher resolution images of C8-BTBT on MoS_2/EG further reveal two chiral structures that have not been observed previously (Figure 2c,d), although they are expected based on the geometry of individual C8-BTBT molecules. The two chiral molecular arrangements are shown schematically at the bottom of Figure 2c,d.

Although the point defect density of CVD-grown rotationally commensurate MoS_2 on EG is almost an order of magnitude smaller than that of MoS_2 grown on amorphous oxide substrates,[26] point defects are still present and appear as local protrusions and depressions in STM imaging as shown in Figure S3a. In addition, protruding point defects are commonly observed on bare EG surfaces after graphitization of SiC in UHV (Figure S3b). As shown in Figures 2e,f, and S2c–e, 1L C8-BTBT self-assembles conformably and continuously across both protruding (blue arrows) and depressed (white arrow) point defects without being perturbed. Furthermore, 1L C8-BTBT molecular stripes seamlessly extend across the step edges of single EG layers (Figure S3e). This relative insensitivity to substrate surface defects leads to low defect density in 1L C8-BTBT, which is a highly desirable property for obtaining highly ordered C8-BTBT monolayers with well-defined organic–inorganic interfaces in addition to serving as templates for subsequent surface chemistry.

Since CVD-grown MoS_2 adopts triangular domain shapes, the crystallographic orientation of MoS_2 can be inferred even when the atomic lattices cannot be resolved through the C8-BTBT adlayers. Even though MoS_2 possesses 3-fold symmetry, 1L C8-BTBT on MoS_2 typically forms a single crystalline domain. If we define the acute angle between the C8-BTBT stripe orientation (red lines) and the MoS_2 domain edge as α (inset of Figure 3a), this angle is found to consistently average ~68° across 19 domains, as shown in Figure 3a, indicating preferred registry of the C8-BTBT molecules on MoS_2. If the triangular MoS_2 domains are assumed to have Mo-terminated edges, the relative orientation of 1L C8-BTBT can be deduced as schematically shown in Figure 3b. Due to the lack of lattice matching between C8-BTBT and MoS_2, there is no specific translational lattice registry between the two. Together with the predictable GB orientations (30° and 60°) of MoS_2 resulting from its rotational commensurability on EG,[26] the rotational registry of 1L C8-BTBT on MoS_2 renders the types of GBs in 1L C8-BTBT substantially limited. For instance, Figure 3c–e show STM images of 1L C8-BTBT self-assembled across the commonly observed 30° and 60° GBs for MoS_2 and a rarely observed 21.1° MoS_2 GB, respectively. The orientation of 1L C8-BTBT in each case is indicated by the white dashed lines, and schematically shown in the insets, in agreement with the above-determined angle of α. Especially, for the 21.1° GB in Figure 3e, the expected relative angle between adjacent C8-BTBT domains is 22.9°, in close agreement with the measured angle of 23.8°. In Figure 3d, the orientations of C8-BTBT are different on the three layers of MoS_2, but still agree with the model in Figure 3b. Although MoS_2 GBs are known to present additional electronic features that decay into each domain over a length scale (~3–4 nm) larger than the size of an individual C8-BTBT molecule,[26] the molecules assemble and join abruptly at the GBs as shown in the inset of Figure 3e. This result again demonstrates the high tolerance of C8-BTBT self-assembly with respect to substrate inhomogeneities, presumably due to strong inter-molecular interactions in C8-BTBT monolayers, in contrast to site-specific self-assembly of molecules on textured surfaces.[33,34] In contrast, for 1L C8-BTBT on EG, different domains are expected to rotate by 60° in accordance with the 6-fold symmetry of the EG surface (Figure S4a). Indeed, a similar approach as was described above for 1L C8-BTBT on MoS_2 was used to deduce the relative orientation of 1L C8-BTBT on EG, which is in agreement with computational modeling (Figure S3b–d).[24]

I_t–V_s measurements and differential tunneling conductance plots, which are proportional to the local density of states, of 1L C8-BTBT on EG and MoS_2 are shown in Figure 4a,b, respectively. When the bias voltage is swept inside and outside

DOI: 10.1021/acs.chemmater.8b05348
Chem. Mater. 2019, 31, 1761–1766

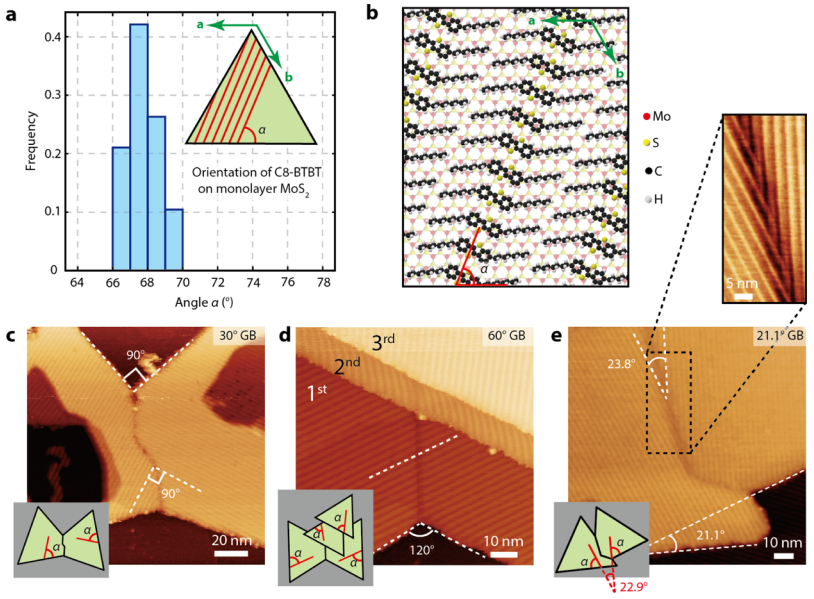

Figure 3. (a) Distribution of α defined by the relative acute angle between the edge of a MoS_2 domain and the stripe orientation of 1L C8-BTBT (red lines). (b) Schematic illustration of the orientation of 1L C8-BTBT on MoS_2. (c–e) STM images of (c) 30°, (d) 60°, and (e) 21.1° GBs of MoS_2 covered by 1L C8-BTBT and schematic illustrations, respectively. In d, the layer-numbers of the MoS_2 are labeled. Inset in e: a zoomed-in STM image of the interface region.

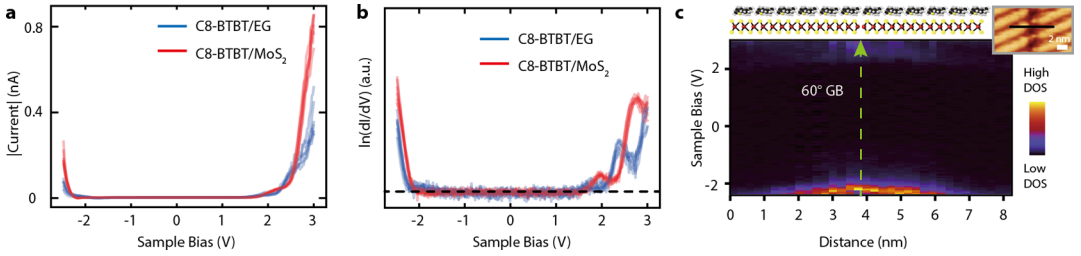

Figure 4. (a) I_t–V_s and (b) STS spectra (semi-log) of 1L C8-BTBT on EG and MoS_2 (measured at 6 positions on each region). The black dashed line in (b) indicates the noise floor. (c) Differential tunneling conductance from a series of STS spectra taken across a 60° GB of MoS_2 covered by 1L C8-BTBT (inset).

the gap, the fact that the respective tunneling current reaches the noise floor (~0 pA) and hundreds of pA suggests that the tip-sample distance is at an appropriate value for this set point condition (V_s = 2.3 V, I_t = 40 pA). In both regions, the STS spectra (Figure 4b) shown on a semi-log plot reveal a bandgap of ~4 eV, which is consistent with expectations for C8-BTBT. No significant tip induced band bending effects are observed under these measurement conditions (Figure S5). Since the Fermi level lies near the center of the gap, the STS spectra suggest an intrinsic semiconducting behavior instead of the p-type character reported for C8-BTBT thin-film transistors measured in ambient conditions.[20,21] This difference can likely be explained by the complete free carrier depletion of 1L C8-BTBT when interfaced with n-type MoS_2 or n-type EG[35] due to the small thickness of the molecular layer. In addition, atmospheric exposure is known to p-type dope thin-film transistors due to the electron withdrawing character of adsorbed oxygen,[36] unlike the present samples that are fully prepared and measured in UHV. By performing a series of STS measurements across a GB of 1L C8-BTBT that resides over a 60° MoS_2 GB (Figure 4c inset), the gap size is observed to decrease by ~0.3 eV at the GB interface. This value is significantly smaller than the ~1.5 eV band gap reduction that was previously measured for a bare 60° MoS_2 GB,[26] which implies that 1L C8-BTBT can effectively screen the local electronic states of the underlying MoS_2.

In summary, we have shown that C8-BTBT forms well-defined interfaces with monolayer MoS_2 in UHV. Furthermore, we demonstrated the fabrication of atomically pristine C8-BTBT/MoS_2/EG mixed-dimensional heterostructures with all components obtained from bottom-up growth that is compatible with large-area processing. The self-assembled monolayer structure of C8-BTBT on MoS_2 has been characterized by molecular-resolution STM imaging, and is shown to be rotationally commensurate with the underlying MoS_2/EG substrate. In addition, the self-assembly of C8-BTBT on MoS_2/EG is insensitive to substrate structural defects and electronic perturbations, implying strong intermolecular interactions and relatively weak molecule–substrate coupling. Overall, this work establishes C8-BTBT/MoS_2/EG as a well-defined, rotationally-commensurate mixed-dimensional heterostructure that can be fabricated over large-areas as is needed for ongoing efforts related to organic/TMDC electronic, optoelectronic, and photovoltaic device technologies.

DOI: 10.1021/acs.chemmater.8b05348
Chem. Mater. 2019, 31, 1761–1766

■ ASSOCIATED CONTENT

Supporting Information

The Supporting Information is available free of charge on the ACS Publications website at DOI: 10.1021/acs.chemmater.8b05348.

Additional experimental methods, additional AFM images, STM images of C8-BTBT over defects, and orientations of C8-BTBT on EG (PDF)

■ AUTHOR INFORMATION

Corresponding Author

*E-mail: m-hersam@northwestern.edu.

ORCID

Xiaolong Liu: 0000-0002-6186-5257
Itamar Balla: 0000-0002-9358-5743
Vinod K. Sangwan: 0000-0002-5623-5285
Hakan Usta: 0000-0002-0618-1979
Antonio Facchetti: 0000-0002-8175-7958
Tobin J. Marks: 0000-0001-8771-0141
Mark C. Hersam: 0000-0003-4120-1426

Author Contributions

This manuscript was written through contributions of all authors.

Notes

The authors declare no competing financial interest.

■ ACKNOWLEDGMENTS

We acknowledge support from the Office of Naval Research (ONR N00014-17-1-2993) and the National Science Foundation Materials Research Science and Engineering Center (NSF DMR-1720139). CVD growth of MoS_2 was supported by the National Institute of Standards and Technology (NIST CHiMaD 70NANB14H012). X.L. further acknowledges support from a Ryan Fellowship that is administered through the Northwestern University International Institute for Nanotechnology.

■ REFERENCES

(1) Liu, X.; Hersam, M. C. Interface Characterization and Control of 2D Materials and Heterostructures. *Adv. Mater.* **2018**, *30*, 1801586.

(2) Jariwala, D.; Marks, T. J.; Hersam, M. C. Mixed-Dimensional van der Waals Heterostructures. *Nat. Nanotechnol.* **2016**, *16*, 170−181.

(3) Sangwan, V. K.; Hersam, M. C. Electronic Transport in Two-Dimensional Materials. *Annu. Rev. Phys. Chem.* **2018**, *69*, 299−325.

(4) Zheng, Y. J.; Huang, Y. L.; Chen, Y.; Zhao, W.; Eda, G.; Spataru, C. D.; Zhang, W.; Chang, Y.-H.; Li, L.-J.; Chi, D.; Quek, S. Y.; Wee, A. T. S. Heterointerface Screening Effects Between Organic Monolayers and Monolayer Transition Metal Dichalcogenides. *ACS Nano* **2016**, *10*, 2476−2484.

(5) Choi, J.; Zhang, H.; Choi, J. H. Modulating Optoelectronic Properties of Two-Dimensional Transition Metal Dichalcogenide Semiconductors by Photoinduced Charge Transfer. *ACS Nano* **2016**, *10*, 1671−1680.

(6) Jariwala, D.; Sangwan, V. K.; Wu, C.-C.; Prabhumirashi, P. L.; Geier, M. L.; Marks, T. J.; Lauhon, L. J.; Hersam, M. C. Gate-Tunable Carbon Nanotube-MoS_2 Heterojunction p-n Diode. *Proc. Natl. Acad. Sci. U.S.A.* **2013**, *110*, 18076−18080.

(7) Shastry, T. A.; Balla, I.; Bergeron, H.; Amsterdam, S. H.; Marks, T. J.; Hersam, M. C. Mutual Photoluminescence Quenching and Photovoltaic Effect in Large-Area Single-Layer MoS_2−Polymer Heterojunctions. *ACS Nano* **2016**, *10*, 10573−10579.

(8) Zang, H.; Routh, P. K.; Huang, Y.; Chen, J.-S.; Sutter, E.; Sutter, P.; Cotlet, M. Nonradiative Energy Transfer From Individual CdSe/ZnS Quantum Dots to Single-Layer and Few-Layer Tin Disulfide. *ACS Nano* **2016**, *10*, 4790−4796.

(9) Li, P.; Yuan, K.; Lin, D.-Y.; Xu, X.; Wang, Y.; Wan, Y.; Yu, H.; Zhang, K.; Ye, Y.; Dai, L. A Mixed-Dimensional Light-Emitting Diode Based on a p-MoS_2 Nanosheet and an n-CdSe Nanowire. *Nanoscale* **2017**, *9*, 18175−18179.

(10) Sangwan, V. K.; Jariwala, D.; Filippone, S. A.; Karmel, H. J.; Johns, J. E.; Alaboson, J. M. P.; Marks, T. J.; Lauhon, L. J.; Hersam, M. C. Quantitatively Enhanced Reliability and Uniformity of High-K Dielectrics on Graphene Enabled by Self-Assembled Seeding Layers. *Nano Lett.* **2013**, *13*, 1162−1167.

(11) Wang, H.; Liu, F.; Fu, W.; Fang, Z.; Zhou, W.; Liu, Z. Two-Dimensional Heterostructures: Fabrication, Characterization, and Application. *Nanoscale* **2014**, *6*, 12250−12272.

(12) Liu, X.; Balla, I.; Bergeron, H.; Campbell, G. P.; Bedzyk, M. J.; Hersam, M. C. Rotationally Commensurate Growth of MoS_2 On Epitaxial Graphene. *ACS Nano* **2015**, *10*, 1067−1075.

(13) Zhang, Z.; Chen, P.; Duan, X.; Zang, K.; Luo, J.; Duan, X. Robust Epitaxial Growth of Two-Dimensional Heterostructures, Multiheterostructures, and Superlattices. *Science* **2017**, *357*, 788−792.

(14) Wang, S.; Wang, X.; Warner, J. H. All Chemical Vapor Deposition Growth of MoS_2:h-BN Vertical van der Waals Heterostructures. *ACS Nano* **2015**, *9*, 5246−5254.

(15) Mouri, S.; Miyauchi, Y.; Matsuda, K. Tunable Photoluminescence of Monolayer MoS_2 via Chemical Doping. *Nano Lett.* **2013**, *13*, 5944−5948.

(16) Jariwala, D.; Howell, S. L.; Chen, K.-S.; Kang, J.; Sangwan, V. K.; Filippone, S. A.; Turrisi, R.; Marks, T. J.; Lauhon, L. J.; Hersam, M. C. Hybrid, Gate-Tunable, van der Waals p-n Heterojunctions from Pentacene and MoS_2. *Nano Lett.* **2015**, *16*, 497−503.

(17) Liu, X.; Gu, J.; Ding, K.; Fan, D.; Hu, X.; Tseng, Y.-W.; Lee, Y.-H.; Menon, V.; Forrest, S. R. Photoresponse of an Organic Semiconductor/Two-Dimensional Transition Metal Dichalcogenide Heterojunction. *Nano Lett.* **2017**, *17*, 3176−3181.

(18) Homan, S. B.; Sangwan, V. K.; Balla, I.; Bergeron, H.; Weiss, E. A.; Hersam, M. C. Ultrafast Exciton Dissociation and Long-Lived Charge Separation in a Photovoltaic Pentacene-MoS_2 van der Waals Heterojunction. *Nano Lett.* **2016**, *17*, 164−169.

(19) Hong, X.; Kim, J.; Shi, S.-F.; Zhang, Y.; Jin, C.; Sun, Y.; Tongay, S.; Wu, J.; Zhang, Y.; Wang, F. Ultrafast Charge Transfer in Atomically Thin MoS_2/WS_2 Heterostructures. *Nat. Nanotechnol.* **2014**, *9*, 682−686.

(20) Yuan, Y.; Giri, G.; Ayzner, A. L.; Zoombelt, A. P.; Mannsfeld, S. C. B.; Chen, J.; Nordlund, D.; Toney, M. F.; Huang, J.; Bao, Z. Ultra-High Mobility Transparent Organic Thin Film Transistors Grown by an Off-Centre Spin-Coating Method. *Nat. Commun.* **2014**, *5*, 3005.

(21) Minemawari, H.; Yamada, T.; Matsui, H.; Tsutsumi, J. y.; Haas, S.; Chiba, R.; Kumai, R.; Hasegawa, T. Inkjet Printing of Single-Crystal Films. *Nature* **2011**, *475*, 364−367.

(22) Zhang, Y.; Qiao, J.; Gao, S.; Hu, F.; He, D.; Wu, B.; Yang, Z.; Xu, B.; Li, Y.; Shi, Y.; Ji, W.; Wang, P.; Wang, X.; Xiao, M.; Xu, H.; Xu, J.-B.; Wang, X. Probing Carrier Transport and Structure-Property Relationship of Highly Ordered Organic Semiconductors at the Two-Dimensional Limit. *Phys. Rev. Lett.* **2016**, *116*, 016602.

(23) Xu, R.; He, D.; Zhang, Y.; Wu, B.; Liu, F.; Meng, L.; Liu, J.-F.; Wu, Q.; Shi, Y.; Wang, J.; Nie, J.-C.; Wang, X.; He, L. Unveiling the Structural Origin of the High Carrier Mobility of a Molecular Monolayer on Boron Nitride. *Phys. Rev. B* **2014**, *90*, 224106.

(24) He, D.; Zhang, Y.; Wu, Q.; Xu, R.; Nan, H.; Liu, J.; Yao, J.; Wang, Z.; Yuan, S.; Li, Y.; Shi, Y.; Wang, J.; Ni, Z.; He, L.; Miao, F.; Song, F.; Xu, H.; Watanabe, K.; Taniguchi, T.; Xu, J.-B.; Wang, X. Two-Dimensional Quasi-Freestanding Molecular Crystals for High-Performance Organic Field-Effect Transistors. *Nat. Commun.* **2014**, *5*, 5162.

(25) Wu, B.; Zhao, Y.; Nan, H.; Yang, Z.; Zhang, Y.; Zhao, H.; He, D.; Jiang, Z.; Liu, X.; Li, Y.; Shi, Y.; Ni, Z.; Wang, J.; Xu, J.-B.; Wang, X. Precise, Self-Limited Epitaxy of Ultrathin Organic Semiconductors and Heterojunctions Tailored by van der Waals Interactions. *Nano Lett.* **2016**, *16*, 3754−3759.

DOI: 10.1021/acs.chemmater.8b05348
Chem. Mater. 2019, 31, 1761−1766

(26) Liu, X.; Balla, I.; Bergeron, H.; Hersam, M. C. Point Defects and Grain Boundaries in Rotationally Commensurate MoS_2 on Epitaxial Graphene. *J. Phys. Chem. C* **2016**, *120*, 20798−20805.
(27) Withers, F.; Del Pozo-Zamudio, O.; Mishchenko, A.; Rooney, A. P.; Gholinia, A.; Watanabe, K.; Taniguchi, T.; Haigh, S. J.; Geim, A. K.; Tartakovskii, A. I.; Novoselov, K. S. Light-Emitting Diodes by Band-Structure Engineering in van der Waals Heterostructures. *Nat. Mater.* **2015**, *14*, 301−306.
(28) Furchi, M. M.; Pospischil, A.; Libisch, F.; Burgdörfer, J.; Mueller, T. Photovoltaic Effect in an Electrically Tunable van der Waals Heterojunction. *Nano Lett.* **2014**, *14*, 4785−4791.
(29) Lee, C.-H.; Lee, G.-H.; van der Zande, A. M.; Chen, W.; Li, Y.; Han, M.; Cui, X.; Arefe, G.; Nuckolls, C.; Heinz, T. F.; Guo, J.; Hone, J.; Kim, P. Atomically Thin P-N Junctions with van der Waals Heterointerfaces. *Nat. Nanotechnol.* **2014**, *9*, 676−681.
(30) Liu, X.; Wei, Z.; Balla, I.; Mannix, A. J.; Guisinger, N. P.; Luijten, E.; Hersam, M. C. Self-Assembly of Electronically Abrupt Borophene/Organic Lateral Heterostructures. *Sci. Adv.* **2017**, *3*, e1602356.
(31) Ueno, K.; Sasaki, K.; Nakahara, T.; Koma, A. Fabrication of C_{60} Nanostructures by Selective Growth on GaSe/MoS_2 and InSe/MoS_2 Heterostructure Substrates. *Appl. Surf. Sci.* **1998**, *130−132*, 670−675.
(32) He, D.; Pan, Y.; Nan, H.; Gu, S.; Yang, Z.; Wu, B.; Luo, X.; Xu, B.; Zhang, Y.; Li, Y.; Ni, Z.; Wang, B.; Zhu, J.; Chai, Y.; Shi, Y.; Wang, X. A van der Waals p-n Heterojunction with Organic/Inorganic Semiconductors. *Appl. Phys. Lett.* **2015**, *107*, 183103.
(33) Mao, J.; Zhang, H.; Jiang, Y.; Pan, Y.; Gao, M.; Xiao, W.; Gao, H.-J. Tunability of Supramolecular Kagome Lattices of Magnetic Phthalocyanines Using Graphene-Based Moire Patterns as Templates. *J. Am. Chem. Soc.* **2009**, *131*, 14136−14137.
(34) Lin, X.; Lu, J. C.; Shao, Y.; Zhang, Y. Y.; Wu, X.; Pan, J. B.; Gao, L.; Zhu, S. Y.; Qian, K.; Zhang, Y. F.; Bao, D. L.; Li, L. F.; Wang, Y. Q.; Liu, Z. L.; Sun, J. T.; Lei, T.; Liu, C.; Wang, J. O.; Ibrahim, K.; Leonard, D. N.; Zhou, W.; Guo, H. M.; Wang, Y. L.; Du, S. X.; Pantelides, S. T.; Gao, H. J. Intrinsically Patterned Two-Dimensional Materials for Selective Adsorption of Molecules and Nanoclusters. *Nat. Mater.* **2017**, *16*, 717−721.
(35) Coletti, C.; Riedl, C.; Lee, D. S.; Krauss, B.; Patthey, L.; von Klitzing, K.; Smet, J. H.; Starke, U. Charge Neutrality and Band-Gap Tuning of Epitaxial Graphene on SiC by Molecular Doping. *Phys. Rev. B* **2010**, *81*, 235401.
(36) Piazza, A.; Giannazzo, F.; Buscarino, G.; Fisichella, G.; Magna, A. L.; Roccaforte, F.; Cannas, M.; Gelardi, F. M.; Agnello, S. Graphene p-Type Doping and Stability by Thermal Treatments in Molecular Oxygen Controlled Atmosphere. *J. Phys. Chem. C* **2015**, *119*, 22718−22723.

DOI: 10.1021/acs.chemmater.8b05348
Chem. Mater. 2019, 31, 1761−1766